PHYSICS

Observation of the quantum phase of free fall and the consistency with the equivalence principle

Or Dobkowski[1], Barak Trok[1], Peter Skakunenko[1], Yonathan Japha[1], David Groswasser[1], Maxim Efremov[2,3], Chiara Marletto[4], Ivette Fuentes Guridi[5,6], Roger Penrose[7], Vlatko Vedral[4], Wolfgang P. Schleich[3,8], Ron Folman[1]*

The unification of quantum theory and the general theory of relativity, describing gravity, is one of the most important challenges in science. Einstein's general theory of relativity is based on the principle of equivalence and has been confirmed to great accuracy for large bodies. However, in the quantum domain, the equivalence principle has been predicted to take a unique form involving a gauge phase, which is equal, in the context of a measurement on Earth, to the quantum phase of a free-falling wave packet relative to its counterpart wave packet which is static in Earth's frame. To measure this phase, we realize a novel cold-atom interferometer in which one wave packet stays static in the laboratory frame while the other is in free fall. The observed relative phase of the wave packets confirms the predicted phase and shows that, in our low energy regime, the equivalence principle may be applied to the quantum domain. Our observation constitutes a fundamental test of the interface between quantum theory and gravity. The new interferometer also opens the door for further probing of the latter interface, as well as to searches for new physics.

INTRODUCTION

The two pillars of 20th century physics—quantum mechanics (QM) and general relativity (GR)—have long stood side by side, resisting all attempts to bring them convincingly together. Related to the latter, ever since Galileo and Newton, it was clear that the phenomenon of free fall in a gravitational field is a paradigm of physics and must be fully understood as part of any description of nature. Einstein went a step further and used the geometry of space-time to describe gravity and free fall. An additional outcome of GR is that one should be able to describe nature from different frames of reference. Rooted in Galileo's insight and elevated by Einstein to a foundational axiom, the principle of equivalence has guided our understanding of gravitation for over a century (*1*–*4*). The rise of QM has not changed any of these convictions. The connection between these two pillars of modern physics remains one of the most important open questions in physics, and it is thus of paramount importance to understand the phenomenon of free fall and the equivalence principle (EP) also in the quantum domain.

The phase of a free-falling wave packet (WP) relative to a WP static in the Earth's frame is predicted in a purely quantum manner to have a dependence $m/\hbar\left(g^2T^3/6+gzT\right)$ on the free-fall time T, where m is the mass of the object, g is the gravitational acceleration relative to the surface of Earth, and z is the spatial coordinate in the direction of gravity. This prediction follows the calculated phase accumulated by an object accelerating in a linear potential and has been made starting from almost 100 years ago by Darwin, Kennard, and others (*5*–*13*). Alternatively, one may derive this phase in a completely different manner, specifically using the EP and a Galilean transformation. The identity of the outcome of the two calculations may be seen as what allows QM and the EP to coexist. Numerous authors have suggested that this phase has implications regarding the EP in the quantum domain (*3*, *8*, *14*–*16*). Remarkably, this crucial phase has never been measured.

Matter-wave quantum interferometers are high-precision tools capable of measuring global and relative accelerations. Interferometry in the presence of the gravitational field of Earth has been previously achieved with neutrons in the celebrated Colella-Overhauser-Werner (COW) experiment (*17*, *18*) [as well as by Bonse and Wroblewski for a noninertial frame (*19*)] and with atoms (*20*–*22*), where the gravitational acceleration g (*23*–*26*) and the gravitational constant G (*27*, *28*) have been measured, but as noted, the explicit phase of a free-falling WP with respect to Earth has not been directly measured.

Here, we report the measurement of the quantum phase of an object in free fall (in the sense that the experimentalist does not apply any forces to it), as observed in a frame stationary with respect to Earth. A direct measurement of this phase requires a unique interferometer using a superposition of one WP in free fall and another WP stationary in Earth's frame. We have named this interferometer the quantum Galileo interferometer, or QGI, in honor of Galileo's discoveries regarding the laws of free fall. Figure 1A describes such a Gedanken (thought) experiment, where the WP that is at rest in the laboratory (Earth) frame is termed the "reference WP," while the WP that is free falling in this frame is termed the "ballistic WP."

While a cubic phase dependence on the interferometer time may also appear in a few situations that are not related to a linear gravitational potential (*29*–*32*), a specific example being the measurement of the curvature in the gravitational field of a test mass [(*33*, *34*); see

[1]Department of Physics and Ilse Katz Institute for Nanoscale Science and Technology, Ben-Gurion University of the Negev, Be'er Sheva 84105, Israel. [2]German Aerospace Center (DLR), Institute of Quantum Technologies, 89081 Ulm, Germany. [3]Institut für Quantenphysik and Center for Integrated Quantum Science and Technology (IQST), Universität Ulm, 89081 Ulm, Germany. [4]Clarendon Laboratory, University of Oxford, Parks Road, Oxford OX1 3PU, UK. [5]School of Physics and Astronomy, University of Southampton, Southampton SO17 1BJ, UK. [6]Keble College, University of Oxford, Oxford OX1 3PG, UK. [7]Mathematical Institute, Andrew Wiles Building, University of Oxford, Radcliffe Observatory Quarter, Woodstock Road, Oxford OX2 6GG, UK. [8]Hagler Institute for Advanced Study at Texas A&M University, Texas A&M AgriLife Research, Institute for Quantum Science and Engineering (IQSE), and Department of Physics and Astronomy, Texas A&M University, College Station, TX 77843-4242, USA.
*Corresponding author. Email: folman@bgu.ac.il

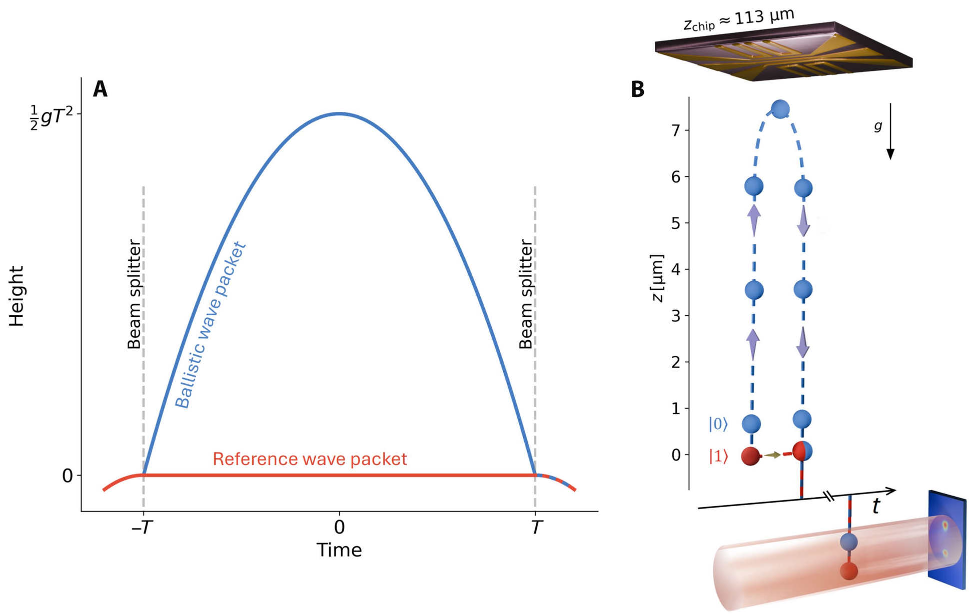

Fig. 1. The QGI experiment to measure the phase accumulation of a free-falling particle. (**A**) Space-time diagram illustrating the classical trajectories of the WPs in the interferometer. A beam splitter creates a coherent superposition of two WPs with different spin states, launching one WP into a freely falling ballistic trajectory for a duration of $2T$, while the second WP is held stationary, serving as a reference. A second beam splitter recombines the two WPs at the end of the ballistic trajectory. State-dependent detection (not shown) measures the population in each state, revealing the phase difference between the two trajectories. (**B**) A schematic of our experimental realization: In the longitudinal (1D) QGI interferometer, the stationary WP is held against gravity using magnetic gradients produced by currents in microfabricated wires on the atom chip. This WP, associated with state $|1\rangle \equiv |F=2, m_F=1\rangle$ of a ^{87}Rb atom, is positioned $\approx 113\ \mu m$ below the chip surface. The ballistic WP, associated with state $|0\rangle \equiv |F=1, m_F=0\rangle$, travels upward reaching, in this example, a splitting of about $7.5\ \mu m$ (about seven times the WP size; see the Supplementary Materials). Interchanging currents in the three central wires (shown in the figure) create a two-dimensional quadrupole to realize a strong magnetic gradient with a small magnetic field, which minimizes phase noise. Last, to measure the population in each spin state, another (reversed) magnetic gradient separates the two states in position so that they can be imaged by a CCD. See Materials and Methods for more details.

Supplementary Materials], observing the cubic phase due to free fall in the QGI configuration constitutes a direct test and confirmation of the relative phase acquired by a free-falling object and, as noted, of the predicted phase when applying the EP to a quantum WP in free fall. Specifically, none of the previous experiments measuring a T^3 behavior have had in the two interferometer arms the accelerations of 0 and g with respect to Earth, and consequently, none measured the predicted prefactor of $\frac{m}{6}g^2/\hbar$. As explained in the following, this requires a hybrid interferometer to be realized, a very different configuration from the latter interferometers.

To briefly show how the same phase is predicted by the EP, we will assume that the EP holds in the quantum domain and calculate the observable consequence of such an assumption. To begin with, throughout this work, we assume the equality of the inertial mass (m_i) and the gravitational mass (m_g), such that $m_i = m_g = m$, as suggested by Galileo and confirmed experimentally with early experiments by Newton, Bessel, and Eötvös and more recent experiments with improved accuracy (*35–38*). We of course also assume the universality of free fall to hold, so that also a ^{87}Rb atom in free fall accelerates toward Earth with acceleration g.

We now view the experiment from two frames of reference, one in free fall and one static relative to Earth. These two frames may be referred to as the Einsteinian and the Newtonian frames, respectively (*15*). The transformation between the wave function ψ_N in a Newtonian (laboratory) frame of reference, where the acceleration of a free object is denoted as $\ddot{z} = -g$, and the wave function ψ_E of the same object in an Einsteinian frame that free-falls with the same acceleration $-g$, and when at $t = 0$ both have the same velocity, involves a transformation phase which may also be referred to as a gauge phase ϕ_{gauge} (*16*). This gauge phase may be calculated by using Galilean transformations (see Supplementary Materials).

If one then assumes that the inertial mass is equal to the gravitational mass, this transformation phase takes the form [e.g., (*15*, *16*)]

$$\psi_N(z,t) = e^{i\phi_{\text{gauge}}(z,t)}\psi_E\left(z + g\frac{t^2}{2}, t\right), \text{ where } \phi_{\text{gauge}} = \frac{m}{\hbar}\left(-\frac{1}{6}g^2t^3 - gzt\right) \quad (1)$$

According to the EP, ψ_E is the wave function of a free particle that feels no forces in the free-falling (Einsteinian) frame (see the Supplementary Materials). Hence, if one assumes that the EP holds, then this WP does not accumulate any phase (beyond free evolution). However, Eq. 1 implies that such a wave function accumulates a phase ϕ_{gauge} in the laboratory (Newtonian) frame, simply due to the transformation between frames.

In conclusion, when comparing a quantum state in two different descriptions—one in which the gravitational field is treated as an external force and another adopting the freely falling frame—a unique phase factor emerges, $mg^2t^3/6\hbar$ (*3*, *8*, *14–16*). This contribution, first identified nearly a century ago as the phase of a freely falling object, has since attracted considerable theoretical scrutiny (*5–13*). However, while this phase was typically calculated as the phase of an accelerating particle, without regard for the problem of the interplay between QM and GR, remarkably, as highlighted by numerous works (3, 8, 14–16), without this phase QM and the EP do not coexist. Specifically, by using the EP, as we did above, one predicts the same phase. In the case that the quantum calculation of an accelerating object under gravity, as was calculated by the numerous authors, was not complete, or in case the application of the EP to the quantum domain, as we have done, is lacking, it is of paramount importance to experimentally confirm this phase. We emphasize that, in this work, we will not be excluding all possible models for which the EP does not hold, as such models may also predict the same phase. Assuming that the EP holds and observing no contradiction, we are able to show that the EP may be applied to a quantum WP. Hence, beyond the measurement of the phase of a free-falling quantum object, the QGI enables the observation of the phase enabling the coexistence of QM and the EP.

RESULTS

Experiment

Our experiment intended to measure this phase—by way of interference with a reference WP—follows the Gedanken experiment presented in Fig. 1A where, at time $t = t_0$, the WP is split into two paths where in one path it is at rest in the Newtonian frame, due to an applied levitating force that is exactly opposite to gravity (hereafter levitation condition), while in the other path, it is in free fall, namely, at rest in the freely falling Einsteinian frame. To achieve recombination of the two paths, the WP in the freely falling path is initially launched upward by a magnetic-gradient pulse with a velocity v_0 in the direction opposite to gravity and then falls freely for a time $2T = 2v_0/g$ (hereafter closing condition), after which an identical magnetic-gradient pulse erases the velocity difference between the two WPs so that the two paths overlap in position and momentum.

For an intuitive understanding of the QGI phase in the Newtonian frame, we fix the reference WP center at vertical position $z = 0$ so that it does not accumulate any propagation phase (beyond the free evolution of the WP) and calculate the phase accumulated by the ballistic WP. As noted, the latter accumulates no propagation phase in the freely falling (Einsteinian) frame, so that the phase at the center of the ballistic WP in the Newtonian frame is nothing but the gauge phase. The phase of the ballistic path is the difference between the phase of the WP center at the two path endpoints, which is equal to the gauge phase at these points. Taking the middle of the path to be at time $t = 0$, these endpoints are at $t = \pm T$, where the WP is centered at $z = 0$ after a free-fall duration T with respect to $t = 0$ (Fig. 1A). The gauge phase at the endpoints and the phase of the ballistic path then read

$$\phi_{\text{gauge}}(\pm T) = \mp \frac{m}{6\hbar} g^2 T^3; \phi_{\text{ballistic}} = \phi_{\text{gauge}}(T) - \phi_{\text{gauge}}(-T) = -2 \cdot \frac{m}{6\hbar} g^2 T^3 \quad (2)$$

As $\phi_{\text{reference}} = 0$, it follows that $\phi_{\text{ballistic}}$ is the relative phase observed in the experiment (see the Supplementary Materials). This phase is of course equal to the action of the ballistic path in the Newtonian frame or equivalently of the reference path in the Einsteinian frame, as we show in the Supplementary Materials. In the Supplementary Materials, we also show that it can be calculated using the Galilean transformation. Note also that the linear term in Eq. 1 vanishes when the endpoints are at $z = 0$, and even if the levitation condition is not satisfied, it is cancelled by the magnetic gradient pulses, which are necessary for the closing condition (see the Supplementary Materials).

Beyond the above description of the fundamental uniqueness of the QGI, in which the measured phase is equal to the free-fall phase, its technical distinctiveness should also be emphasized. While the Ramsey-Bordé interferometer is mostly characterized by the constant spatial separation between the two interferometer paths (39), and the Kasevich-Chu interferometer is mostly characterized by the piece-wise constant velocity separation (difference) between the two paths (40), the QGI enables the control of all degrees of freedom, obtaining spatial, velocity, and acceleration differences, almost at will. This allowed us to have one WP at rest and the other free falling. Furthermore, typical atom interferometers are free-space interferometers, whereby during most of their motion, the WPs do not experience any potential applied by the experimental setup (41). Some interferometers do have a potential applied to both WPs during their evolution, and these may be termed guided interferometers (42, 43). In our case, both methods are used simultaneously, one for each of the WPs. The QGI is thus a hybrid interferometer.

Experimental scheme

In Fig. 1B, we present the experimental setting in which the QGI, using ^{87}Rb atoms, is conducted about 113 μm below an atom chip (44), where the current-carrying wires give rise to the magnetic field gradients which are responsible for the Stern-Gerlach (SG) type forces applied to the WPs. The QGI is a novel type of SG interferometer (SGI), leveraging a decade of SGI experiments in which the necessary techniques were developed (45), and, consequently, is now capable of demonstrating enhanced stability, larger phase accumulation, and especially the flexibility required to enable one WP to take a ballistic trajectory while the other is stationary.

During the free-fall time, the ballistic WP is in state $|0\rangle \equiv |F=1, m_F=0\rangle$, so that to first order in the Zeeman interaction it is not affected by the magnetic gradients. The reference WP is in state $|1\rangle \equiv |F=2, m_F=1\rangle$ and is held vertically stationary in the laboratory frame (i.e., relative to Earth) by a "holding magnetic gradient pulse" producing a magnetic acceleration a in the opposite direction to gravity, holding or levitating the WP in a constant vertical position. Both states belong to the atomic ground state, whereby F is the total angular momentum of an atomic state and m_F is its projection on the quantization axis. The acceleration a is independently tuned by an experimental procedure (see Materials and Methods and the Supplementary Materials) to satisfy the levitation condition for which the reference WP is stationary. In case of small experimental errors, one can consider the general case that includes deviations from the levitation condition, for which a simple calculation of the actions along the two interferometer trajectories when the closing condition is satisfied results in a measured QGI phase

$$\Delta\phi = \frac{ma(a-2g)}{3\hbar} T^3 \quad (3)$$

such that the outcome of the QGI depends on both the applied external acceleration on the reference arm and the free-fall acceleration and becomes equal to the result of Eq. 2 in the case $a = g$, with a quadratic deviation $m(a-g)^2 T^3/3\hbar$ if $a \neq g$. While the measurement of g is not the aim of our experiment, we should note that the sensitivity with which a T^3 SGI, such as ours, can measure g was recently estimated (46).

The momentum splitting of the WPs in the experiment requires a finite kick duration T_{kick} in which the reference WP is temporarily in state $|0\rangle$ and the ballistic WP is temporarily in state $|1\rangle$ allowing it to be accelerated with an average acceleration $a_{\text{kick}} = v_0 / T_{\text{kick}}$. Furthermore, to perform the internal-state flip before or after the kick, a finite delay time T_{d} is needed between the kick pulse and the holding pulse of duration $T_{\text{h}} = 2T - 2T_{\text{d}}$, where $2T$ represents the free-fall time of the ballistic WP. As explained in Materials and Methods, the ballistic WP has a free-fall time of $2T$, while the reference WP is in free fall during the time $T_{\text{kick}} + T_{\text{d}}$ before and after the holding time. Using ϕ_{gauge}, these latter parts of the reference WP trajectory involve a free-fall phase in the laboratory (Newtonian) frame of

$$\phi_{\text{reference}} = \frac{2m}{3\hbar} g^2 \left(T_{\text{kick}} + T_{\text{d}}\right)^3 \tag{4}$$

Consequently, the phase of the reference WP is independent of the holding time.

By using arguments similar to the ones used above to derive the previous equations, we can also calculate the phase of the ballistic WP during the kick time and obtain the total phase difference expected in the experiment (see the Supplementary Materials)

$$\Delta\phi = \frac{mg^2}{3\hbar}\left[T^3 + T^2 T_{\text{kick}} + T\left(T_{\text{kick}}^2 + T_{\text{kick}} T_{\text{d}}\right) - T_{\text{d}}\left(T_{\text{kick}} + T_{\text{d}}\right)^2\right] \tag{5}$$

where the quadratic and linear dependence on the interferometer time T is due to the finite duration of the kick T_{kick} (setting $T_{\text{kick}} = 0$ eliminates them), while T_{d} adds a constant phase term.

Let us briefly describe in more detail the experimental sequence we have realized (more details in Materials and Methods and the Supplementary Materials): We create a Bose-Einstein condensate (BEC) consisting of about $2 \cdot 10^4$ atoms in a magnetic trap, using current-carrying wires on an atom chip (the atoms are below the chip which is upside down; Fig. 1B). We then release the atom cloud from the trap and conduct a Delta-kick cooling (DKC; collimation) procedure. The atom cloud is by now dilute enough so that atom-atom interaction is minimized and the physics becomes essentially single-particle physics. After a $\pi/2$ pulse, each atom is in a superposition of a magnetic sensitive state $|1\rangle$ and a nonsensitive state $|0\rangle$.

Next, we apply a magnetic kick which launches state $|1\rangle$ upward. Quickly thereafter, we apply a π pulse, so that the WP launched upward is in state $|0\rangle$ and is no longer affected by the magnetic gradients, thus going into a ballistic trajectory affected only by gravity (up to second-order Zeeman).

Conversely, the other WP, which is now in state $|1\rangle$, is sensitive to the magnetic gradient which is at this time tuned so that it exactly counteracts gravity. Consequently, this WP remains static and does not change position. Last, we reverse the sequence to bring the two WPs to have the same position and momentum for a full overlap.

The detection stage starts with a $\pi/2$ pulse which projects the phase difference between the spin states to the population of the states. Next, another magnetic gradient kick separates the two spin states in space, so that after some time of flight, we are able to determine the population in each spin state using absorption imaging with a charge-coupled device (CCD) and thus measure the output of the interferometer.

Beyond the achievement of two very different WP trajectories in space, a substantial experimental challenge lies in the fact that the two trajectories are very much different in momentum, and recombining the WPs to observe an interference pattern requires a good overlap in both position and momentum (namely, zeroing any difference or, in other words, time reversing the splitting process). The time irreversibility of the splitting process, whether it be of technical or fundamental origin, has been termed by Scully, Englert, and Schwinger the "Humpty-Dumpty effect," and combating it requires precise control over the trajectories (*47*).

More so, for a good overlap, the size and shape of the two WPs have to be quite similar, and as they are exposed to different magnetic gradients having a different curvature, lensing effects make such an overlap hard to achieve. Last, also rotation of the WPs in three-dimensional may diminish the eventual overlap and consequently the contrast (visibility) of the interference pattern (*48*).

Whereas recombination in atom interferometers based on laser pulses, even when the momentum splitting is large (*49*), enjoys the naturally given quantum accuracy of the photon momentum, in an SGI, the momentum transfer is classical in nature. This requires a high level of control over the magnetic fields as well as a detailed simulation of the WP evolution when exposed to such fields and gravity (*50*).

Measurements

In Fig. 2, we present the raw data, where we observe about 13 oscillations, which constitute about 80 rad phase accumulation. To obtain the fit, we first identify the upper and lower envelopes and fit them to a polynomial to get P_{mean} and $V(2T)$. We then fit the data to the model where the phase $\phi(2T)$ is a third-order polynomial. During the fitting, we exclude the first and last oscillations as they suffer from larger uncertainty in the values of the envelope. The data show 13 complete oscillations, with low phase noise, resulting in an average population error (SEM) of 1.8 ± 1.5 [%] and good visibility, starting at $V = 80\%$ and decreasing to $V = 20\%$ at $2T = 2000\,\mu\text{s}$. The decrease in visibility is mainly due to a varying overlap between the WPs due to differences in shape evolution under the influence of curved gradients as well as imperfection in the path recombination. The figure includes 633 experimental cycles, each 30 s, so the graph was taken over a period of 5.3 hours. The short-term and long-term stability of the interferometer are good due to the high stability of the chip trap and current source.

In Fig. 3, we analyze the phase extracted from Fig. 2 and compare it to a numerical simulation (green dots), the analytical prediction of Eq. 5 (blue dashed), as well as to the Gedanken experiment of Eq. 2 (black dashed). The analytical model assumes a homogeneous magnetic gradient along the z axis and a set of square pulses of current so that the acceleration of each arm is a piecewise constant function, giving rise to a purely one-dimensional motion along z, which, together with the symmetry of the scheme, results in perfect path recombination. The numerical simulation is based on tools we developed for calculating WP evolution in curved potentials (*50*), which include the effects of shape and rotation of the WP on the phase and visibility of the interferometer. The numerical simulation takes into account (i) three-dimensional propagation in a curved potential resulting in a nonperfect path recombination, (ii) internal WP dynamics (expansion, focusing, and rotation), and (iii) atom-atom interactions within each WP. The first two factors may change the phase by an order of 1 to 2 rad each, while the latter may contribute up to about 0.25 rad. Obviously, the prediction of the numerical simulation is accurate to within the uncertainty limits of the experimental parameters.

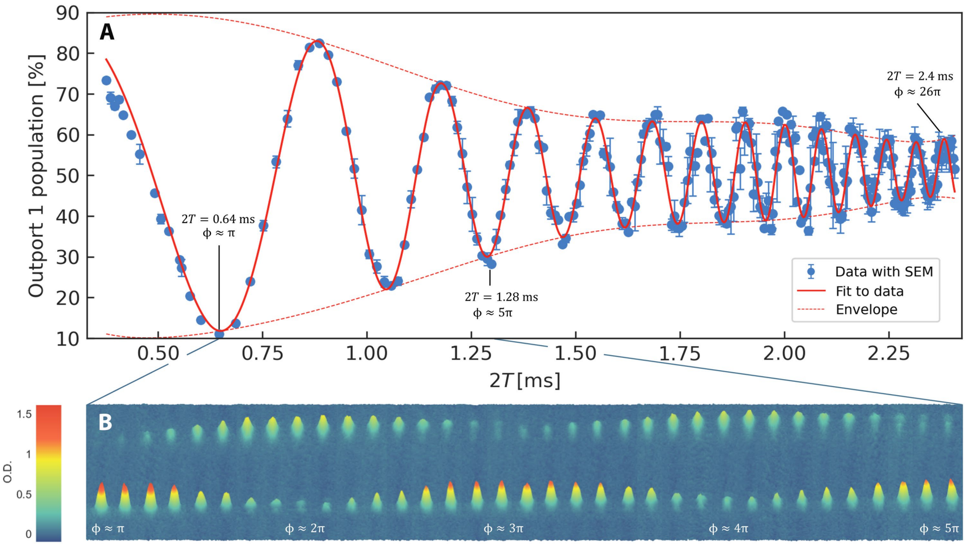

Fig. 2. Population in outport 1 versus the free-fall duration of the ballistic path 2*T*. (**A**) The relative spin population in outport 1 (state $|0\rangle$) oscillates with a distinct chirp as a function of interferometer time. The blue points represent the experimental data, with error bars derived from the SEM. The red line is a fit to the data of the form $P = P_{\text{mean}}(2T) + \frac{1}{2}V(2T)\cos[\phi(2T)]$, where V is the visibility of the oscillations, ϕ is the phase of the oscillations, and P_{mean} is the mean value of the population. See text for more details. (**B**) Atomic distribution (heatmap of optical density) taken from CCD images (on-resonance absorption imaging), of the atoms in the two interferometer outports (see Fig. 1B), showing two oscillations. The top cloud is outport 1 (state $|0\rangle$), and the bottom cloud is outport 2 (state $|1\rangle$, which is magnetically sensitive). The cloud in outport 2 is focused by the final splitting pulse, increasing its optical density and making it appear slightly denser even when the two clouds have the same population. The vertical scale of the image is 1.1 mm.

As can be seen from Fig. 3B, the residuals amount to about 2.5%, presenting good agreement between the model and the data for the T^3 term.

The inset of Fig. 3A shows the derivative of the phase with respect to $2T$. To obtain the derivative of the phase for the numeric simulation, we fit a third-order polynomial to the set of points in the main figure and take its derivative. The derivative of the analytical approximation and the Gedanken experiment are calculated by direct differentiation.

Last, we compare the experimental results to possible deviations from the model. The yellow dashed lines in Fig. 3A represent 5% deviations from the T^3 phase accumulation model, by modifying the analytical prediction to a power law of $T^{3\pm0.15}$, which demonstrates that the data exclude such deviations from the T^3 phase accumulation. The thin blue dashed lines represent the analytical approximation with 5% deviations from the theoretical prefactor (note that the prefactor in our experiment is $mg^2/3\hbar$, as explained in Eq. 2). The data are consistent with the predicted value of the $mg^2/6\hbar$ prefactor (see Introduction), as shown in Fig. 3C.

In the Supplementary Materials, we provide detailed information as to how all lines in Figs. 2 and 3 were plotted. The main source of uncertainty in the experimental results arises from the systematic uncertainty in the ratio of the kick and holding currents, as the phase accumulation is most sensitive to this ratio, where deviations from the desired ratio add a phase term that scales linearly with the interferometer time.

DISCUSSION

The good agreement between the data and the analytical as well as numerical prediction brings us to conclude that we have observed the expected interferometer phase difference of $-\frac{m}{3\hbar}g^2t^3$ (Eq. 2), and in doing so, we have confirmed with a high level of confidence the predicted $-\frac{m}{6\hbar}g^2t^3$ phase (Eq. 1). We have thus observed the phase of a freely falling object.

Although measuring g is clearly not the goal of our experiment, the phase of a freely falling object is proportional to g so the measurement of the phase may be considered a measurement of gravity. Measuring gravity has been done for hundreds of years, and ever since the celebrated COW experiments (*17*, *18*), also with matter-wave interferometers. Last, for the past three decades, measuring gravity has been done also with atom interferometers such as ours (*20*–*26*), and it has already become part of technology (*51*–*54*), but one should nevertheless acknowledge subtleties. Specifically, it is agreed that the EP indicates that all tests of fundamental physics (including gravitational physics) are not affected, locally, by the presence of a gravitational field (*55*). One may interpret this to mean that matter-wave interferometers cannot measure gravity in the absolute sense in a uniform gravitational field, but it is understood that if a part of the apparatus is firmly connected to Earth (the source mass), then this constitutes nonlocal position information (i.e., instantaneous relative position between the measuring apparatus and source mass), and gravity may be measured (*56*).

In the QGI, this information is transferred from the apparatus to the reference WP, by the levitation condition. More explicitly, the position of the reference WP, as well as the apparatus, is fixed relative to the surface of Earth, located at a distance $r = R$ from the center of Earth ($r = 0$), and hence ignoring rotations and tidal movements has the same acceleration as the center of Earth, $g(r = 0)$, which may have a nonzero value due to some external gravitational field (e.g., from the Sun). The free-falling WP experiences $g(R)$, which, in addition to $g(0)$, is due to the gravitational pull of Earth, again ignoring rotations and tidal movements. The relative acceleration of the two WPs is thus determined by the gravity of Earth.

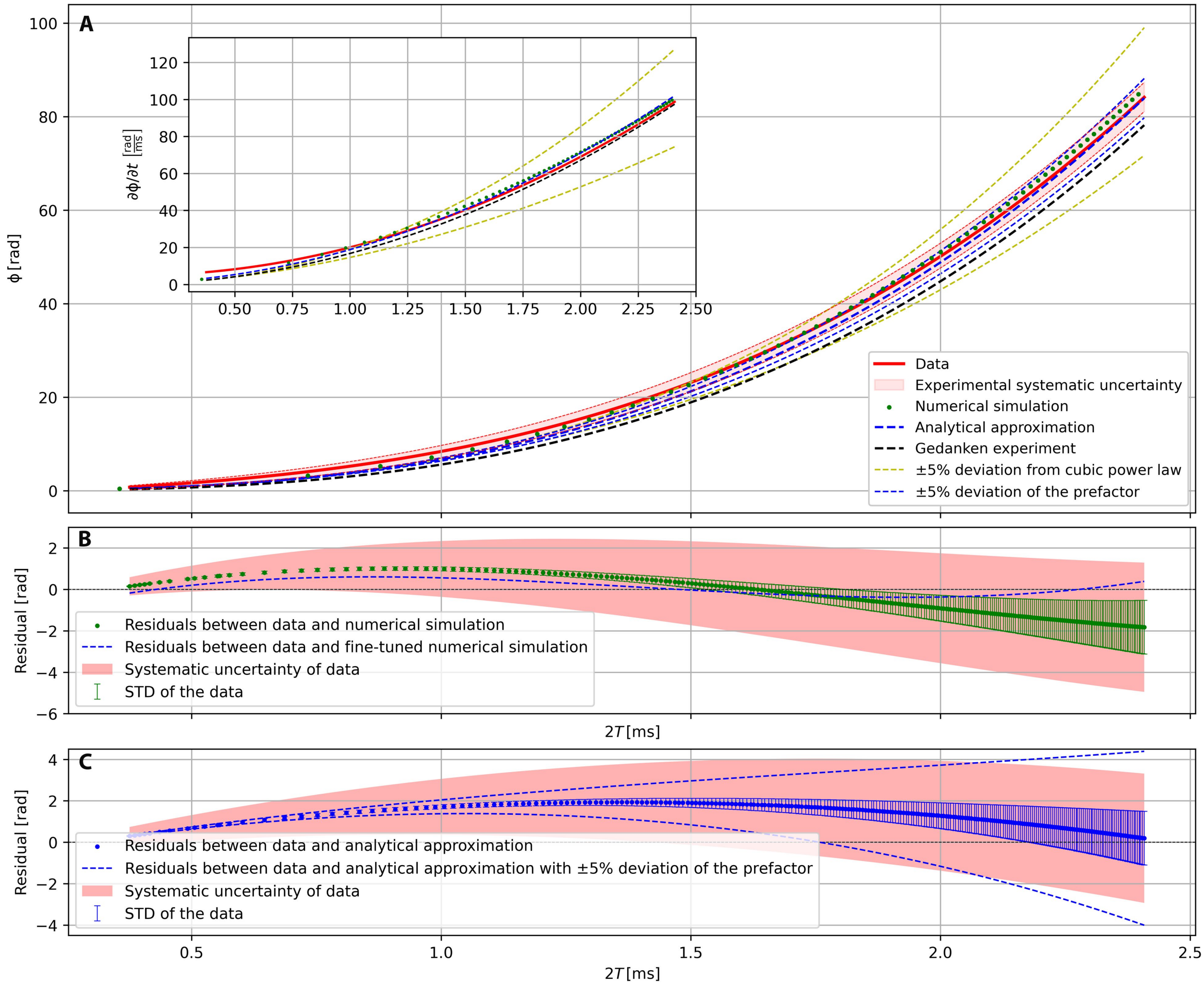

Fig. 3. Phase and its derivative versus the free-fall duration of the ballistic path 2*T*. (**A**) The phase difference between the two interferometer arms as a function of the free-fall duration of the upper arm. The red line represents the experimental data, where the phase is extracted from Fig. 2. To estimate the uncertainty bounds, we repeat the experiment with an increase (decrease) of the magnetic-pulse current I_{kick} by 0.5% (which is our estimated experimental precision) and use the result to plot the upper (lower) uncertainty bounds. The green dots and thick dashed lines represent the theoretical predictions. The thin dashed lines are meant to show that the data exclude such deviations from the cubic phase or the predicted prefactor. See text for details. (**B**) The residuals between the phase of the data and the numerical simulation, where the latter is a "blind" simulation with no free parameters or fine tuning. A difference of 2 rad over 13 oscillations spanning a phase of ≈ 80 rad constitutes a deviation of about 2.5%. The error bars represent the statistical noise of the phase in the experiment, which shows a relative noise of 1.3% of the phase. The red band represents the systematic uncertainties [which also appear in (A)]. The blue line shows the result of the numeric simulation after fine-tuning of the currents and the magnetic field along the *z* axis. The kick current is increased by 0.15%, the idle current is changed from 0.55 to 0.5 mA, and B_z is changed from 0.33 to 0.35 G, all within the experimental uncertainties. (**C**) The residuals between the phase of the data and the analytical approximation. The 5% lines allow one to put an upper limit of a few percent on the possible deviation from the predicted prefactor.

The QGI has a unique geometry which allows to directly measure the phase of a free-falling WP due to gravity. Obviously, observing from the Einsteinian frame, the observer may claim that the phase is due to the magnetic acceleration, but this is of course also a measure of gravity due to the levitation condition, which determines the equality

$$\Delta\phi = -\frac{(mg)^2 T^3}{3\hbar m} = -\frac{F_{\mathrm{mag}}^2 T^3}{3\hbar m} \tag{6}$$

To conclude, we have measured the quantum phase of a freely falling object, by comparing its free-falling WP to its counterpart WP—static in the Earth's frame, and at the same time, we have confirmed the phase predicted if the EP is applied to a freely falling WP. Nature, it seems, at these low masses and energies, does accommodate both QM and the EP in this delicate manner. In the outlook, we look beyond the present work and consider how future versions of the experiment may draw us into even deeper waters. In this light, the present experiment may be seen not merely as a confirmation of a long-predicted quantum phase but as a potential stepping stone toward a deeper synthesis of gravity and quantum theory.

As an outlook, let us introduce the term quantum equivalence principle (QEP). As there seems to be no agreement on how to exactly define the QEP, we leave this for future theoretical and experimental work (*14*, *16*, *57*–*64*). Quite a few works claim that the t^3

phase is also a fundamental aspect of the EP for quantum systems (*3*, *8*, *14*, *16*). Hence, it may be argued that the QGI experiment described here also observed a consequence of the QEP. Other, more complex tests are also being suggested (*65*).

Let us note two final points: First, as the QGI is also able to manipulate clock WPs [for clocks in an SGI, see (*66*)], it opens the door for the test of the more complex formulations suggested for the EP in the quantum domain. Such an interferometer also opens the door to searches for new physics with clocks (*67*–*71*). Second, such an interferometer is a milestone toward an SGI with nanodiamonds instead of atoms, for a test of QM in new regimes and to probe the quantum-gravity interface (*72*), e.g., test the quantization of gravity (*47*, *73*, *74*). In addition, such a large-mass (active-mass) interferometer can explore the Díosi-Penrose conjecture regarding gravitationally induced collapse and possible tensions which may arise with the QEP (see the Supplementary Materials) (*75*–*77*).

MATERIALS AND METHODS

Let us describe the experimental sequence in some detail (see Fig. 4 for the entire experimental scheme and Fig. 5 for a zoom-in on the interferometer scheme): We create a ^{87}Rb BEC in the state $|2\rangle \equiv |F=2, m_F=2\rangle$ in a magnetic trap produced by current-carrying wires on the atom chip (below the chip which is upside down). We then release the cloud of atoms from the trap and conduct DKC, which collimates the expansion of the WP along the z axis down to an effective temperature of 3.3 nK. As a side effect of this procedure, the atoms are launched upward (as can be seen on the left side of Fig. 4). The BEC is by now dilute enough so that atom-atom interaction is minimized and the physics becomes single-atom physics. We then apply 100-μs radio frequency (RF) π pulse transferring atoms to the state $|F=2, m_F=1\rangle$. With the help of a microwave (MW) $\pi/2$ pulse, each atom is now in a superposition of a magnetic sensitive state $|1\rangle \equiv |F=2, m_F=1\rangle$ and a nonsensitive state $|0\rangle \equiv |F=1, m_F=0\rangle$. We now apply a magnetic SG kick which launches the sensitive state upward. Quickly thereafter, we apply a MW π pulse, so that the atoms launched upward are no longer affected by the magnetic gradients and they go into a ballistic trajectory affected only by gravity (up to second-order Zeeman). Conversely, the other WP becomes sensitive to the magnetic gradient which is now tuned to exactly counteract gravity, so that the WP remains stationary in the frame of reference of the laboratory. Last, we reverse the sequence—apply a MW π pulse and apply the same SG kick to stop the ballistic WP, thus bringing the two WPs to have the same position and momentum for a full overlap. After one more MW $\pi/2$ pulse, another magnetic gradient kick separates the two spin states in space, so that after some time of flight, we are able to determine the population in each output port and consequently in each spin state and thus measure the output of the interferometer (Fig. 2).

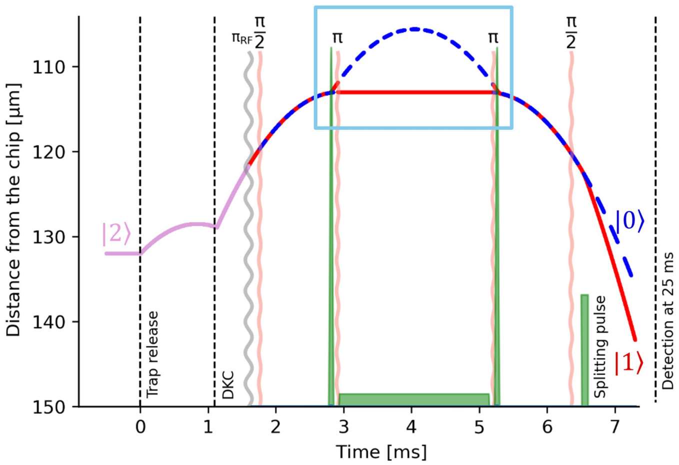

Fig. 4. The experimental scheme and trajectories of the WPs in the experiment. The complete experimental scheme of our longitudinal (1D) QGI, for the case of $2T = 2.4$ ms. We set $t = 0$ at the moment of trap release. At this time, the atoms are in the state $|2\rangle \equiv |F=2, m_F=2\rangle$. We apply DKC at $t = 1.1$ ms, which collimates the WP's expansion and launches the atoms into a ballistic trajectory upward. Before the start of the interferometer, we transfer the atoms to the state $|1\rangle \equiv |F=2, m_F=1\rangle$ by applying an on-resonance RF π pulse (gray wavy line). During the interferometer, we control the spin state of the atoms with four MW pulses (orange wavy lines) and the momentum of the atoms with three magnetic gradient pulses (green areas). The MW pulses are on resonance with the transition between the $|1\rangle$ and $|0\rangle \equiv |F=1, m_F=0\rangle$ states, where the $|0\rangle$ state is magnetically nonsensitive in the Zeeman first order. The first $\pi/2$ pulse puts the atoms in an equal superposition of $|1\rangle + |0\rangle$. At the end of the interferometer, the trajectories of these two states are joined to a single trajectory with two spin states, after which the second $\pi/2$ pulse is applied, creating four overlapping WPs which interfere, two WPs per each spin state, imprinting the phase difference into a population difference (for simplicity of graphics, we have not differentiated the four WPs in the plot). After the second $\pi/2$ pulse, we detect the relative population in each state. In the detection scheme, we first spatially separate the states by applying a fourth magnetic gradient and, lastly, image the atoms using on-resonance absorption imaging. The blue frame emphasizes the interferometer stage and is explained in Fig. 5.

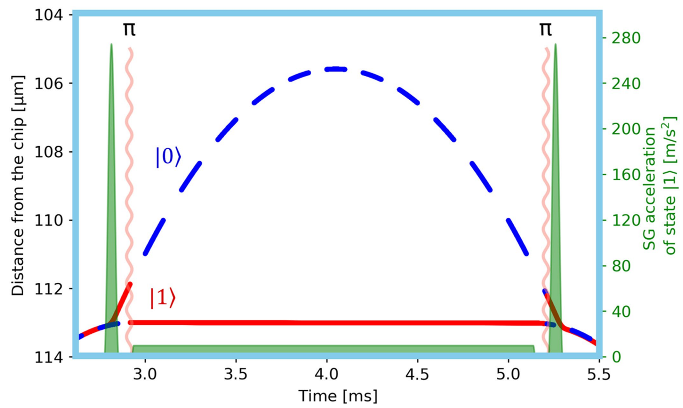

Fig. 5. The interferometer scheme and trajectories of the WPs in the experiment. Zoom-in on the interferometer sequence (the blue frame is the same one shown in Fig. 4). The first gradient (kick) pulse applies a maximal acceleration a_{kick} for a total duration of T_{kick}, which launches the top arm into a ballistic trajectory. Fifty microseconds after the end of the gradient pulse, we apply a π pulse (with a duration of 16 μs) that inverts the spin state of the arms so that the bottom arm is now in the magnetically sensitive state $|1\rangle$. Five microseconds after the π pulse, we start the holding pulse (duration of T_{h} and rise time $\tau_{\text{h}} = 12$ μs), which applies an acceleration opposite and equal to gravity, to hold the bottom arm stationary in the laboratory frame. Fifty microseconds after the holding pulse, we again apply a π pulse, and 5 μs later, we recombine the trajectories of the two WPs by applying a magnetic gradient pulse with a maximal acceleration a_{kick} for a total duration of T_{kick}, as in the first pulse. For the interferometer to work, the symmetric timing of the $\pi/2$ and π pulses serves as a dynamic decoupling scheme, increasing the coherence time, canceling the linear phase accumulation due to possible detuning of the MW, and reducing the shot-to-shot phase fluctuations.

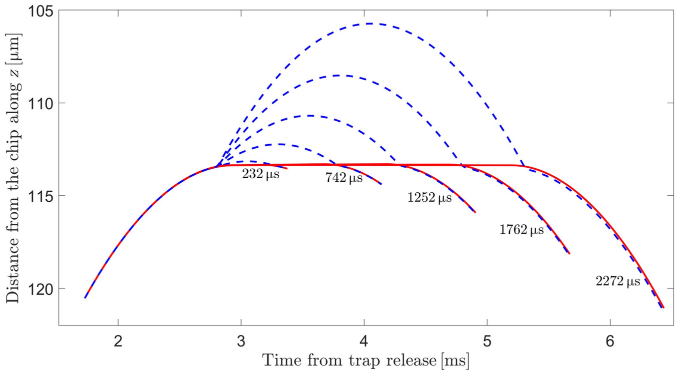

Fig. 6. The trajectories of the WPs for different holding durations. The trajectories of the two arms of the interferometer, calculated by the numerical simulation for holding durations $T_h = 232,742,1252,1762,2272\,\mu s$. Blue dashed lines represent the ballistic trajectory, and red solid lines represent the static WP. At the end of the interferometer, a small spatial splitting can be seen, on the order of 0.1 μm For $T_h = 2272\,\mu s$, the spatial splitting between the two arms halfway through the interferometer reaches 7.5 μm. The trajectories are plotted until the time in which the second (and final) $\pi/2$ is applied.

The SG force is created by currents in three parallel gold microwires of 2-μm thickness, 40-μm width, separated by 60-μm gaps on the atom chip surface. The current direction in the middle wire is opposite to that in the edge wires, which creates a quadrupole magnetic field with a minimum at ∼100 μm from the wires. The external magnetic bias field of 12.6 G is applied to suppress spin-flips and introduce a small second-order Zeeman shift for the efficiency of the RF pulse.

The optimal value of the holding current I_{hold} should counteract gravity. To find I_{hold}, we measured trajectories of state $|1\rangle$ with resonant absorption imaging for various values of the holding current (see the Supplementary Materials for details) and find $I_{hold} = 23.07 \pm 1.49$ mA. Although the inaccuracy of gravity compensation is 6.5%, it corresponds to only 0.42% inaccuracy in the phase accumulation, as the deviation from g is introduced squared to the phase (see the Supplementary Materials). We note that the phase of Eq. 3 has a maximum value at $a = g$ which reduces the sensitivity to small changes of the magnetic acceleration while keeping the sensitivity to the gravitational acceleration linear.

The kick currents are set in such a way that the area $\int I(t)dt$ of the two kick current pulses is equal to the area of the holding current pulse for each interferometer duration. In the case of the Gedanken experiment and the analytical approximation, such a definition of the kick pulses is equivalent to the condition of full overlap between the WPs at the end of the interferometer. However, in the real experiment, this condition does not result in perfect overlap due to the curvature of the potential and the finite duration of the pulses. This is quantified in the numerical simulation, where the precise pulse area condition is applied, and the two trajectories do not completely overlap at the end, resulting in a small final spatial splitting of 0.2 μm for the largest interferometer duration (as seen in Fig. 6). The effects of rotations and the expansion of the WPs under the curved potential are also quantified in the numerical simulation and contribute up to 1 rad to the total phase (as seen in fig. S4). While in Fig. 4 the trajectories are produced by an analytical approximation, in Fig. 6, we present several trajectories as they are calculated by the numerical simulation, and as in Fig. 3, the two are in good agreement. The maximal reached spatial splitting between the two arms is ∼7.5 μm, based on the numerical simulation and in agreement with the analytical estimations and trajectory imaging.

Next, let us briefly describe the timings of the MW pulses. We use a symmetric dynamical decoupling MW scheme, as it cancels the linear phase due to possible detuning of the MW pulses, improves the coherence time, and reduces the shot-to-shot noise. The rise and fall time of the holding pulse (duration of T_h) are each defined as $\tau_h = 12\,\mu s$. The time between the first and second π pulses defines the MW dynamical decoupling scheme. We define it as $2\tau_{DD}$, which amounts to $2\tau_{DD} = 5 + 2\times\tau_h + T_h + 50$, where $5\,\mu s$ after the π pulse, we start the holding pulse, and 50 μs after the end of the holding pulse, we apply the second π pulse (Fig. 4). We then set the time between the $\pi/2$ and π pulses to be τ_{DD}.

Last, let us describe with a simplified calculation (details in the Supplementary Materials) how the $T_h = 2272\,\mu s$ (Fig. 6) or the $2T = 2.4\,ms$ (Fig. 4) achieves a splitting of about 7.5 μm. We define T_d as the delay between the end of the gradient (kick) pulse and the start of the holding pulse, where 50 μs after the end of the gradient pulse, we apply a π pulse (with a duration of 16 μs) that inverts the spin state of the arms so that the bottom arm is now in the magnetically sensitive state $|1\rangle$, and 5 μs after the π pulse, we start the holding pulse. This amounts to $T_d = 50 + 16 + 5 = 71\,\mu s$, where the same delay time appears also after the holding pulse. The top arm travels $0.5 \times g_{eff} \times (T_{eff})^2 = 7.62\,\mu m$, where $g_{eff} = 9.91\,m/s^2$ (including acceleration due to the second-order Zeeman shift), and $2T_{eff} = T_h + 2\times\tau_h + 2\times T_d + T_{kick} = 2T + 80\,\mu s$ is the effective ballistic duration taking into account the translation along z during T_{kick} (only one $T_{kick} = 80\,\mu s$ is added as an average of the two kicks). The bottom arm travels upward $0.5 \times g_{eff} \times (T_{kick} + T_d)^2 = 0.11\,\mu m$ during T_{kick} and T_d, resulting in a maximal splitting of 7.5 μm. This is in good agreement with the numerical results presented in Fig. 6. The complete details concerning the experiment may be found in the Supplementary Materials.

Supplementary Materials

This PDF file includes:

Supplementary Text
Figs. S1 to S9
Tables S1 and S2
References

REFERENCES

1. C. C. Speake, C. M. Will, Tests of the weak equivalence principle. *Class. Quantum Grav.* **29**, 180301 (2012).
2. C. M. Will, The confrontation between general relativity and experiment. *Living Rev. Relativ.* **17**, 4 (2014).
3. M. Nauenberg, Einstein's equivalence principle in quantum mechanics revisited. *Am. J. Phys.* **84**, 879–882 (2016).
4. E. Okon, C. Callender, Does quantum mechanics clash with the equivalence principle—and does it matter? *Eur. J. Philos. Sci.* **1**, 133–145 (2011).
5. C. G. Darwin, Free motion in the wave mechanics. *Proc. R. Soc. Lond. A* **117**, 258–293 (1927).
6. E. H. Kennard, Zur Quantenmechanik einfacher Bewegungstypen. *Z. Physik* **44**, 326–352 (1927).
7. E. H. Kennard, The quantum mechanics of an electron or other particle. *J. Franklin Inst.* **207**, 47–78 (1929).
8. D. M. Greenberger, A. W. Overhauser, Coherence effects in neutron diffraction and gravity experiments. *Rev. Mod. Phys.* **51**, 43–78 (1979).
9. H. Beyer, J. Nitsch, The non-relativistic cow experiment in the uniformly accelerated reference frame. *Phys. Lett. B* **182**, 211–215 (1986).

10. R. Penrose, *The Road to Reality*, (Vintage, 2007).
11. R. Penrose, Black holes, quantum theory and cosmology. *J. Phys. Conf. Ser.* **174**, 012001 (2009).
12. R. Penrose, On the gravitization of quantum mechanics 1: Quantum state reduction. *Found. Phys.* **44**, 557–575 (2014).
13. M. Zimmermann, M. A. Efremov, A. Roura, W. P. Schleich, S. A. DeSavage, J. P. Davis, A. Srinivasan, F. A. Narducci, S. A. Werner, E. M. Rasel, T^3-Interferometer for atoms. *Appl. Phys. B* **123**, 102 (2017).
14. F. Giacomini, E. Castro-Ruiz, Č. Brukner, Quantum mechanics and the covariance of physical laws in quantum reference frames. *Nat. Commun.* **10**, 494 (2019).
15. R. Howl, R. Penrose, I. Fuentes, Exploring the unification of quantum theory and general relativity with a Bose–Einstein condensate. *New J. Phys.* **21**, 043047 (2019).
16. C. Marletto, V. Vedral, On the testability of the equivalence principle as a gauge principle detecting the gravitational t^3 phase. *Front. Phys.* **8**, 176 (2020).
17. R. Colella, A. W. Overhauser, S. A. Werner, Observation of gravitationally induced quantum interference. *Phys. Rev. Lett.* **34**, 1472–1474 (1975).
18. H. Rauch, S. A. Werner, *Neutron Interferometry 2nd Edn: Lessons in Experimental Quantum Mechanics, Wave-Particle Duality, and Entanglement* (Oxford Univ. Press, 2015; https://academic.oup.com/book/26204).
19. U. Bonse, T. Wroblewski, Measurement of neutron quantum interference in noninertial frames. *Phys. Rev. Lett.* **51**, 1401–1404 (1983).
20. M. Kasevich, S. Chu, Measurement of the gravitational acceleration of an atom with a light-pulse atom interferometer. *Appl. Phys. B* **54**, 321–332 (1992).
21. G. M. Tino, Testing gravity with cold atom interferometry: Results and prospects. *Quantum Sci. Technol.* **6**, 024014 (2021).
22. S. Lellouch, K. Bongs, M. Holynski, Using atom interferometry to measure gravity. *Contemp. Phys.* **63**, 138–155 (2022).
23. A. Peters, K. Y. Chung, S. Chu, High-precision gravity measurements using atom interferometry. *Metrologia* **38**, 25–61 (2001).
24. L. Zhou, Z.-Y. Xiong, W. Yang, B. Tang, W.-C. Peng, Y.-B. Wang, P. Xu, J. Wang, M.-S. Zhan, Measurement of local gravity via a cold atom interferometer. *Chin. Phys. Lett.* **28**, 013701 (2011).
25. C.-Y. Li, L.-K. Chen, X. Yang, Z.-Y. Xu, M.-Q. Huang, Y. Luo, Y.-H. Zhao, X.-W. Niu, Z.-W. Liu, H.-J. Yao, S. Chen, J.-W. Pan, Drift-free continuous gravity measurement and application analysis of a high-precision atom gravimeter. *Phys. Rev. Appl.* **24**, 014045 (2025).
26. C. Cassens, B. Meyer-Hoppe, E. Rasel, C. Klempt, Entanglement-enhanced atomic gravimeter. *Phys. Rev. X* **15**, 011029 (2025).
27. J. B. Fixler, G. T. Foster, J. M. McGuirk, M. A. Kasevich, Atom interferometer measurement of the newtonian constant of gravity. *Science* **315**, 74–77 (2007).
28. C. D. Panda, M. J. Tao, M. Ceja, J. Khoury, G. M. Tino, H. Müller, Measuring gravitational attraction with a lattice atom interferometer. *Nature* **631**, 515–520 (2024).
29. G. D. McDonald, C. C. N. Kuhn, S. Bennetts, J. E. Debs, K. S. Hardman, J. D. Close, N. P. Robins, A faster scaling in acceleration-sensitive atom interferometers. *EPL* **105**, 63001 (2014).
30. I. Dutta, D. Savoie, B. Fang, B. Venon, C. L. Garrido Alzar, R. Geiger, A. Landragin, Continuous cold-atom inertial sensor with 1 nrad / sec rotation stability. *Phys. Rev. Lett.* **116**, 183003 (2016).
31. G. G. Rozenman, M. Zimmermann, M. A. Efremov, W. P. Schleich, L. Shemer, A. Arie, Amplitude and phase of wave packets in a linear potential. *Phys. Rev. Lett.* **122**, 124302 (2019).
32. O. Amit, Y. Margalit, O. Dobkowski, Z. Zhou, Y. Japha, M. Zimmermann, M. A. Efremov, F. A. Narducci, E. M. Rasel, W. P. Schleich, R. Folman, T^3 stern-gerlach matter-wave interferometer. *Phys. Rev. Lett.* **123**, 083601 (2019).
33. G. Rosi, L. Cacciapuoti, F. Sorrentino, M. Menchetti, M. Prevedelli, G. M. Tino, Measurement of the gravity-field curvature by atom interferometry. *Phys. Rev. Lett.* **114**, 013001 (2015).
34. P. Asenbaum, C. Overstreet, T. Kovachy, D. D. Brown, J. M. Hogan, M. A. Kasevich, Phase shift in an atom interferometer due to spacetime curvature across its wave function. *Phys. Rev. Lett.* **118**, 183602 (2017).
35. T. A. Wagner, S. Schlamminger, J. H. Gundlach, E. G. Adelberger, Torsion-balance tests of the weak equivalence principle. *Class. Quantum Grav.* **29**, 184002 (2012).
36. P. Touboul, G. Métris, M. Rodrigues, Y. André, Q. Baghi, J. Bergé, D. Boulanger, S. Bremer, P. Carle, R. Chhun, B. Christophe, V. Cipolla, T. Damour, P. Danto, H. Dittus, P. Fayet, B. Foulon, C. Gageant, P.-Y. Guidotti, D. Hagedorn, E. Hardy, P.-A. Huynh, H. Inchauspe, P. Kayser, S. Lala, C. Lämmerzahl, V. Lebat, P. Leseur, F. Liorzou, M. List, F. Löffler, I. Panet, B. Pouilloux, P. Prieur, A. Rebray, S. Reynaud, B. Rievers, A. Robert, H. Selig, L. Serron, T. Sumner, N. Tanguy, P. Visser, MICROSCOPE mission: First results of a space test of the equivalence principle. *Phys. Rev. Lett.* **119**, 231101 (2017).
37. G. Rosi, G. D'Amico, L. Cacciapuoti, F. Sorrentino, M. Prevedelli, M. Zych, Č. Brukner, G. M. Tino, Quantum test of the equivalence principle for atoms in coherent superposition of internal energy states. *Nat. Commun.* **8**, 15529 (2017).
38. P. Asenbaum, C. Overstreet, M. Kim, J. Curti, M. A. Kasevich, Atom-interferometric test of the equivalence principle at the 10^{-12} level. *Phys. Rev. Lett.* **125**, 191101 (2020).
39. C. J. Bordé, Atomic interferometry with internal state labelling. *Phys. Lett. A* **140**, 10–12 (1989).
40. M. Kasevich, S. Chu, Atomic interferometry using stimulated Raman transitions. *Phys. Rev. Lett.* **67**, 181–184 (1991).
41. T. Kovachy, P. Asenbaum, C. Overstreet, C. A. Donnelly, S. M. Dickerson, A. Sugarbaker, J. M. Hogan, M. A. Kasevich, Quantum superposition at the half-metre scale. *Nature* **528**, 530–533 (2015).
42. V. Xu, M. Jaffe, C. D. Panda, S. L. Kristensen, L. W. Clark, H. Müller, Probing gravity by holding atoms for 20 seconds. *Science* **366**, 745–749 (2019).
43. K. A. Krzyzanowska, J. Ferreras, C. Ryu, E. C. Samson, M. G. Boshier, Matter-wave analog of a fiber-optic gyroscope. *Phys. Rev. A* **108**, 043305 (2023).
44. M. Keil, O. Amit, S. Zhou, D. Groswasser, Y. Japha, R. Folman, Fifteen years of cold matter on the atom chip: Promise, realizations, and prospects. *J. Mod. Opt.* **63**, 1840–1885 (2016).
45. M. Keil, S. Machluf, Y. Margalit, Z. Zhou, O. Amit, O. Dobkowski, Y. Japha, S. Moukouri, D. Rohrlich, Z. Binstock, Y. Bar-Haim, M. Givon, D. Groswasser, Y. Meir, R. Folman, "Stern-Gerlach interferometry with the atom chip," in *Molecular Beams in Physics and Chemistry*, B. Friedrich, H. Schmidt-Böcking, Eds. (Springer International Publishing, 2021; https://link.springer.com/10.1007/978-3-030-63963-1_14), pp. 263–301.
46. E. Zuniga, E. Gomez, L. O. Castanos-Cervantes, Precision limits of magnetic T^3-atomic gravimetry due to atomic cloud expansion. *Phys. Rev. A* **109**, 013304 (2024).
47. Y. Margalit, O. Dobkowski, Z. Zhou, O. Amit, Y. Japha, S. Moukouri, D. Rohrlich, A. Mazumdar, S. Bose, C. Henkel, R. Folman, Realization of a complete Stern-Gerlach interferometer: Toward a test of quantum gravity. *Sci. Adv.* **7**, eabg2879 (2021).
48. Y. Japha, R. Folman, Quantum uncertainty limit for stern-gerlach interferometry with massive objects. *Phys. Rev. Lett.* **130**, 113602 (2023).
49. J.-N. Kirsten-Siemß, F. Fitzek, C. Schubert, E. M. Rasel, N. Gaaloul, K. Hammerer, Large-momentum-transfer atom interferometers with μrad-accuracy using bragg diffraction. *Phys. Rev. Lett.* **131**, 033602 (2023).
50. Y. Japha, Unified model of matter-wave-packet evolution and application to spatial coherence of atom interferometers. *Phys. Rev. A* **104**, 053310 (2021).
51. X. Wu, Z. Pagel, B. S. Malek, T. H. Nguyen, F. Zi, D. S. Scheirer, H. Müller, Gravity surveys using a mobile atom interferometer. *Sci. Adv.* **5**, eaax0800 (2019).
52. L. Antoni-Micollier, D. Carbone, V. Ménoret, J. Lautier-Gaud, T. King, F. Greco, A. Messina, D. Contrafatto, B. Desruelle, Detecting volcano-related underground mass changes with a quantum gravimeter. *Geophys. Res. Lett.* **49**, e2022GL097814 (2022).
53. C. Janvier, V. Ménoret, B. Desruelle, S. Merlet, A. Landragin, F. Pereira Dos Santos, Compact differential gravimeter at the quantum projection-noise limit. *Phys. Rev. A* **105**, 022801 (2022).
54. J. Fang, W. Wang, Y. Zhou, J. Li, D. Zhang, B. Tang, J. Zhong, J. Hu, F. Zhou, X. Chen, J. Wang, M. Zhan, Classical and atomic gravimetry. *Remote Sens.* **16**, 2634 (2024).
55. E. Di Casola, S. Liberati, S. Sonego, Nonequivalence of equivalence principles. *Am. J. Phys.* **83**, 39–46 (2015).
56. P. Asenbaum, C. Overstreet, M. A. Kasevich, Matter waves and clocks do not observe uniform gravitational fields. *Phys. Scr.* **99**, 046103 (2024).
57. C. Lämmerzahl, On the equivalence principle in quantum theory. *Gen. Relativ. Gravit.* **28**, 1043–1070 (1996).
58. H. C. Rosu, Classical and quantum inertia: A matter of principle. *Gravit. Cosmol.* **5**, 81 (1999).
59. H. Padmanabhan, T. Padmanabhan, Nonrelativistic limit of quantum field theory in inertial and noninertial frames and the principle of equivalence. *Phys. Rev. D* **84**, 085018 (2011).
60. S. T. Pereira, R. M. Angelo, Galilei covariance and Einstein's equivalence principle in quantum reference frames. *Phys. Rev. A* **91**, 022107 (2015).
61. M. Zych, Č. Brukner, Quantum formulation of the Einstein equivalence principle. *Nat. Phys* **14**, 1027–1031 (2018).
62. L. Hardy, Implementation of the quantum equivalence principle. arXiv: 1903.01289 [quant-ph] (2019).
63. S. Das, M. Fridman, G. Lambiase, General formalism of the quantum equivalence principle. *Commun. Phys.* **6**, 198 (2023).
64. F. Giacomini, Č. Brukner, Quantum superposition of spacetimes obeys Einstein's equivalence principle. *AVS Quantum Sci.* **4**, 015601 (2022).
65. R. Geiger, M. Trupke, Proposal for a quantum test of the weak equivalence principle with entangled atomic Species. *Phys. Rev. Lett.* **120**, 043602 (2018).
66. Y. Margalit, Z. Zhou, S. Machluf, D. Rohrlich, Y. Japha, R. Folman, A self-interfering clock as a "which path" witness. *Science* **349**, 1205–1208 (2015).
67. W. P. Schleich, D. M. Greenberger, E. M. Rasel, A representation-free description of the Kasevich–Chu interferometer: A resolution of the redshift controversy. *New J. Phys.* **15**, 013007 (2013).
68. S. Loriani, A. Friedrich, C. Ufrecht, F. Di Pumpo, S. Kleinert, S. Abend, N. Gaaloul, C. Meiners, C. Schubert, D. Tell, É. Wodey, M. Zych, W. Ertmer, A. Roura, D. Schlippert,

W. P. Schleich, E. M. Rasel, E. Giese, Interference of clocks: A quantum twin paradox. *Sci. Adv.* **5**, eaax8966 (2019).
69. E. Giese, A. Friedrich, F. Di Pumpo, A. Roura, W. P. Schleich, D. M. Greenberger, E. M. Rasel, Proper time in atom interferometers: Diffractive versus specular mirrors. *Phys. Rev. A* **99**, 013627 (2019).
70. A. Roura, Gravitational redshift in quantum-clock interferometry. *Phys. Rev. X* **10**, 021014 (2020).
71. F. Di Pumpo, A. Friedrich, C. Ufrecht, E. Giese, Universality-of-clock-rates test using atom interferometry with T^3 scaling. *Phys. Rev. D* **107**, 064007 (2023).
72. C. Marletto, V. Vedral, Quantum-information methods for quantum gravity laboratory-based tests. *Rev. Mod. Phys.* **97**, 015006 (2025).
73. S. Bose, A. Mazumdar, G. W. Morley, H. Ulbricht, M. Toroš, M. Paternostro, A. A. Geraci, P. F. Barker, M. S. Kim, G. Milburn, Spin entanglement witness for quantum gravity. *Phys. Rev. Lett.* **119**, 240401 (2017).
74. C. Marletto, V. Vedral, Gravitationally induced entanglement between two massive particles is sufficient evidence of quantum effects in gravity. *Phys. Rev. Lett.* **119**, 240402 (2017).
75. H. Bondi, Negative mass in general relativity. *Rev. Mod. Phys.* **29**, 423–428 (1957).
76. A. Bassi, K. Lochan, S. Satin, T. P. Singh, H. Ulbricht, Models of wave-function collapse, underlying theories, and experimental tests. *Rev. Mod. Phys.* **85**, 471–527 (2013).
77. S. Bose, I. Fuentes, A. A. Geraci, S. M. Khan, S. Qvarfort, M. Rademacher, M. Rashid, M. Toroš, H. Ulbricht, C. C. Wanjura, Massive quantum systems as interfaces of quantum mechanics and gravity. *Rev. Mod. Phys.* **97**, 015003 (2025).
78. K. A. Whittaker, J. Keaveney, I. G. Hughes, C. S. Adams, Hilbert transform: Applications to atomic spectra. *Phys. Rev. A* **92**, 059904 (2015).
79. G. G. Rozenman, M. Zimmermann, M. A. Efremov, W. P. Schleich, W. B. Case, D. M. Greenberger, L. Shemer, A. Arie, Projectile motion of surface gravity water wave packets: An analogy to quantum mechanics. *Eur. Phys. J. Spec. Top.* **230**, 931–935 (2021).
80. R. DiSalle, *Space and Time: Inertial Frames, The Stanford Encyclopedia of Philosophy, E. N. Zalta Ed*. (Winter 2020 Edition). https://plato.stanford.edu/entries/spacetime-iframes/.

Acknowledgments: We thank the BGU nano-fabrication facility for the high-quality chip and the BGU support team, especially M. Givon, Z. Binstock, D. Kapusta, and Y. Bar-Haim for support in building and maintaining the experiment. We thank Č. Brukner, D. Rohrlich, D. M. Greenberger, E. M. Rasel, Y. Margalit, J. Ströhle, G. G. Rozenman, F. Di Pumpo, and M. Zimmermann for helpful discussions. **Funding:** This work was funded, in part, by the Israel Science Foundation (grants no. 856/18, 1314/19, 3515/20, and 3470/21) and the German-Israeli DIP project (Hybrid devices: FO 703/2-1) supported by the DFG. This work has been supported by the "Table-top experiments for fundamental physics" program, sponsored by the Gordon and Betty Moore Foundation, Simons Foundation, Alfred P. Sloan Foundation, and John Templeton Foundation. I.F.G. thanks an anonymous US philanthropist, J. Moussouris, J. Westergren, and the Emmy Network for support and research funding. C.M. and V.V. thank the Gordon and Betty Moore Foundation and the Templeton Foundation, and C.M. also thanks the Eutopia Foundation and B. Vass for supporting her research. W.P.S. is grateful to the Hagler Institute for Advanced Study at Texas A&M University for a Faculty Fellowship and to Texas A&M AgriLife Research for the support of this work. **Author contributions:** Conceptualization: O.D., B.T., P.S., Y.J., M.E., C.M., I.F.G., R.P., V.V., W.P.S., and R.F. Methodology: O.D., B.T., P.S., Y.J., D.G., M.E., C.M., W.P.S., and R.F. Software: O.D., B.T., P.S., and Y.J. Validation: O.D., B.T., P.S., Y.J., C.M., W.P.S., and R.F. Formal analysis: O.D., B.T., P.S., Y.J., C.M., V.V., W.P.S., and R.F. Investigation: O.D., B.T., P.S., Y.J., D.G., C.M., and R.F. Resources: B.T., P.S., D.G., and R.F. Data curation: B.T., P.S., and Y.J. Writing—original draft: O.D., B.T., Y.J., C.M., I.F.G., W.P.S., and R.F. Writing—review and editing: O.D., B.T., P.S., Y.J., M.E., C.M., I.F.G., R.P., V.V., W.P.S., and R.F. Visualization: O.D., B.T., P.S., W.P.S., and R.F. Supervision: D.G., W.P.S., and R.F. Project administration: B.T., D.G., and R.F. Funding acquisition: R.F. **Competing interests:** The authors declare that they have no competing interests. **Data, code, and materials availability:** All data and code needed to evaluate and reproduce the results in the paper are present in the paper and/or the Supplementary Materials. This study did not generate new materials.

Submitted 3 October 2025
Accepted 24 July 2026
Published 2 September 2026
10.1126/sciadv.aec8045

Science Advances

Observation of the quantum phase of free fall and the consistency with the equivalence principle

Or Dobkowski, Barak Trok, Peter Skakunenko, Yonathan Japha, David Groswasser, Maxim Efremov, Chiara Marletto, Ivette Fuentes Guridi, Roger Penrose, Vlatko Vedral, Wolfgang P. Schleich, and Ron Folman

Sci. Adv. **12** (36), eaec8045. DOI: 10.1126/sciadv.aec8045

Science Advances (ISSN 2375-2548) is published by the American Association for the Advancement of Science. 1200 New York Avenue NW, Washington, DC 20005. The title *Science Advances* is a registered trademark of AAAS.